Cover page

A method to visualize the nanoscopic morphology of astrocytes in vitro and in situ

Janosch P Heller[1,*] and Dmitri A Rusakov[1,2,*]

[1]UCL Institute of Neurology, University College London, Queen Square, London WC1N 3BG, United Kingdom

[2]Laboratory of Brain Microcircuits, Institute of Neuroscience, University of Nizhny Novgorod, Russia.

*Correspondence:

Dmitri Rusakov, email: d.rusakov@ucl.ac.uk

Janosch Heller, email: j.heller@ucl.ac.uk

i. Running head:

Nanoscopy of astrocyte morphology

ii. summary/abstract

In recent years it has become apparent that astroglia are not only essential players in brain development, homeostasis, and metabolic support, but the cells are also essential to the formation and regulation of synaptic circuits. Fine astrocytic processes that can be found in the vicinity of synapses undergo considerable structural plasticity associated with age- and use-dependent changes in neural circuitries. However, due to the extraordinary complex, essentially nanoscopic morphology of astroglia, the underlying cellular mechanisms remain poorly understood.

Here we detail a super-resolution microscopy approach, based on the single-molecule localisation microscopy (SMLM) technique direct stochastic optical reconstruction microscopy (dSTORM) to visualise astroglial morphology on the nanoscale. This approach enables visualisation of key morphological changes that occur in nanoscopic astrocyte processes, whose characteristic size falls below the diffraction limit of conventional optical microscopy.

iii. key words

Super-resolution microscopy, SMLM, dSTORM, brain tissue fixation, tissue sectioning, immunohistochemistry, astrocytes

1. Introduction

Astrocytes play key roles in neurotransmitter uptake and extracellular potassium buffering in the brain. However, as has recently become apparent, the cells also actively contribute to neural circuit formation, maintenance and function. Even though astroglia are electrically non-excitable, they integrate and communicate diverse physiological inputs from brain networks, in health and disease [1-8]. Throughout the brain, nanoscopic astroglial processes (termed perisynaptic astrocytic processes, PAPs) are often found surrounding excitatory synapses where they facilitate intimate astroglia-synapse signal exchange including glutamate transport, potassium buffering, and the release of signalling "gliotransmitter" molecules [9-12,6]. PAP-mediated synapse coverage varies depending on the brain region and on synaptic identity as well as activity [13,14,9,15-19].

Visualising the nanoscopic structure of astrocytes has been technically difficult as the sponge-like astrocytic processes can be as fine as 50-100 nm in diameter, a scale that lies below the diffraction limit of conventional light microscopy (200-300 nm). Historically, electron microscopy (EM) has been the only tool to successfully resolve astroglial structure on the nanoscale [13,20,19,21-24]. However, newly emerging super-resolution microscopy techniques enable imaging of structurally intact cells *in vitro* and *in vivo* at resolution of up to 10-70 nm [25-27]. Through the use of stimulated-emission depletion (STED), photo-activated localization microscopy (PALM) or stochastic optical reconstruction microscopy (STORM) some important aspects of astroglial nano-organization have been revealed already [9,28-33]. Here, we detail a single-molecule localisation microscopy (SMLM) approach based on direct STORM (dSTORM) that uses stochastic excitation of a sparse subset of proteins of interest that are targeted by conventional fluorophore-labelled antibodies [34-36]. With this method we are able to reconstruct fine morphology of astroglia below the diffraction limit of conventional microscopy. We describe the labelling and imaging of the common astroglia marker glial fibrillary acidic protein (GFAP) [37], and the calcium-binding protein S100β [38] which were used previously [39] to reveal the nanostructure of fine astrocytic processes in cultured cells and in fixed brain sections.

2. Materials

Cortical Culture Preparation

1. P0 rats (Sprague Dawley, mixed sex; Charles River, UK).

2. Dissociation Medium (DM): 81.8 mM Na_2SO_4, 30 mM K_2SO_4, 5.8 mM $MgCl_2$, 0.25 mM $CaCl_2$, 1 mM HEPES, 20 mM glucose, 1 mM kynureic acid, 0.001% phenol red. Filtered and stored at 4°C.

3. Digestion medium: DM supplemented with 100 U Papain (Worthington, US-NY). Made fresh on the day.

4. Plating medium: MEM, 10% FBS, 1% Penicilin/Streptomycin, 2 mM GlutaMAX. Filtered and stored at 4°C.

5. Opti-MEM.

6. Centrifuge.

7. 18 mm diameter coverslip (#1.5, scientific laboratory supplies) coated with 1 mg/ml poly-DL-lysine and 25 µg/ml laminin.

8. Maintenance medium: Neurobasal-A w/o Phenol Red, 2% B-27 Supplement, 1% Penicilin/Streptomycin, 0.5 mM Gluta-MAX, 25 µM β-mercaptoethanol. Filtered and stored at 4°C or 37°C.

Brain section preparation

1. P21-28 rats (Sprague Dawley, mixed sex; Charles River, UK).

2. Pentobarbital (100 mg/kg).

3. Perfusion pump system (flow rate: 5 ml/minute) with 26-gauge needle attached.

4. Phosphate-buffered saline (PBS, stored at room temperature).

5. 4% (w/v) paraformaldehyde (PFA, stored at 4°C) in PBS.

6. Vibratome (Leica, #VT1000S).

7. PBS supplemented with 0.01% (w/v) NaN_3 and 100 mM glycine.

Immunochemistry

1. 0.1% (w/v) $NaBH_4$ in PBS. Made fresh on the day.

2. 10 mM $CuSO_4$ in 50 mM NH_4Cl, final pH = 5. Stored at room temperature.

3. PBS-S: 0.2% (w/v) saponin in PBS. Stored at 4°C for several days.

4. Blocking buffer: PBS-S supplemented with 10% (v/v) normal donkey serum.

5. Primary antibodies used can be found in Table 1, and fluorescently-labelled secondary antibodies used are listed in Table 2. Antibodies were diluted in PBS-S supplemented with 2.5% normal donkey serum just before use on the day.

6. TetraSpeck beads (Thermo, #T7279).

7. 4% (w/v) PFA in PBS.

8. Scale U2 buffer (Table 3, stored at 4°C) [40].

Microscopes and sample preparation

1. SMLM-capable microscope: Vutara 350 commercial microscope (Bruker Corp., Billerica, US-MA) based on the SML biplane technology [41,42] with a 60x-magnification, 1.2-NA water immersion objective, a Flash 4.0 scientific complementary metal-oxide semiconductor (sCMOS) camera and a semiconductor charge-coupled devices (CCD) camera.

2. 647 nm (for Alexa647) and 561 nm (for CF568) excitation lasers and a 405 nm activation laser.

3. Photoswitching buffer containing 100 mM cysteamine and oxygen scavengers (glucose oxidase and catalase) (Table 4) [43].

4. Analysis software (Vutara SRX software, version SRX 6.02).

3. Methods

<u>Cortical Culture</u>

Animal procedures were conducted in accord with the European Commission Directive (86/609/ EEC) and the United Kingdom Home Office (Scientific Procedures) Act (1986).

1. The brain was removed from one P0 pup and isolated cortices were placed on ice in DM.

2. Cortices were incubated in digestion medium twice for 15 minutes at 37°C.

3. Cortices were rinsed thrice in DM and thrice in plating medium.

4. Trituration in plating medium until no clumps were visible.

5. Cell solution was diluted 1:10 in Opti-MEM and centrifuged at 1000 rpm for 10 minutes at room temperature.

6. The cell pellet was resuspended in plating medium, cells counted and plated at a density of 150,000 per coverslip.

7. Three hours after plating, medium was exchanged for maintenance medium.

<u>Transcardial perfusion & tissue sectioning</u>

Transcardial perfusion of the animal was used to fix the brain. Good tissue preservation relies on the quality of the perfusion. Animal procedures were conducted in accord with the European Commission Directive (86/609/ EEC) and the United Kingdom Home Office (Scientific Procedures) Act (1986).

1. The animals were terminally anaesthetised with pentobarbital and laid supine.

2. The pleural cavity was exposed, the sternum was lifted away, and the heart was isolated from surrounding connective tissue.

3. The needle was inserted into the left ventricle and clamped with a haemostat. The right atrium was cut and the animal was exsanguinated with 10 ml PBS.

4. The animal was then transcardially perfused with 4% PFA (note 1.), noting the onset of fixation tremors.

5. Then, the brain was removed and post-fixed overnight. Fixed brains can be stored in PBS at 4°C for up to 3 months prior to sectioning.

6. For sectioning, the brain was glued to the vibratome stage using only a little glue, ensuring that no adhesive was in contact with the area to be sectioned.

7. The tissue was then sectioned into 20 μm sections while immersed in PBS.

8. The tissue was either used for imaging immediately or stored for several months at 4°C in PBS with 0.01% (w/v) NaN_3 and 100 mM glycine.

Protocol to label astrocytes in vitro

Unless otherwise stated all procedures were performed at room temperature and under constant, gentle agitation.

1. Fixation of cells with pre-warmed 4% PFA (note 1.) for 10 minutes at 37°C.

2. Washing with PBS thrice (10 minutes each). The cells can be stored in PBS with 0.01% (w/v) NaN_3 and 100 mM glycine for several weeks at 4°C.

3. Quenching with 0.1% $NaBH_4$ (note 1.) in PBS for 7 minutes.

4. Washing with PBS thrice (5 minutes each).

5. Quenching with $CuSO_4$ (10 mM) in NH_4Cl (50 mM), final pH = 5 for 10 minutes.

6. Washing with deionised water quickly, followed by three washes with PBS (5 minutes each).

7. Permeabilisation and blocking with blocking buffer (note 1.) for one hour.

8. Incubation with primary antibody (Table 1, note 2.) solution in PBS-S supplemented with 2.5% donkey serum overnight at 4°C. This incubation step can also be performed at room temperature for 1-2 hours.

9. Washing briefly with PBS-S (~1 minute) and then with blocking buffer thrice (10 minutes each).

10. Incubation with secondary antibody (Table 2, note 2.) solution in PBS-S for 1-2 hours. To avoid bleaching of the fluorophores, the cells have to be shielded from light (for example using aluminium foil to wrap the plate) from this point on.

11. Washing once with PBS-S for 10 minutes.

12. Incubation with fiducial markers (1:500) in PBS for 20 minutes.

13. Washing three times with PBS (10 minutes each).

14. Post fixation with 4% PFA in PBS for 15 minutes.

15. Washing thrice with PBS (10 minutes each).

16. The cells were either imaged immediately or stored in PBS with 0.01% (w/v) NaN_3 for several days.

Protocol to label astrocytes in situ

Unless otherwise stated all procedures were performed at room temperature and under constant, gentle agitation.

1. Free-floating brain sections were briefly washed in PBS to remove any residual PFA.

2. Quenching with 0.1% $NaBH_4$ (note 1.) in PBS for 15 minutes.

3. Washing thrice with PBS (5 minutes each).

4. Quenching with $CuSO_4$ (10 mM) in NH_4Cl (50 mM), final pH = 5 for 10 minutes.

5. Washing with deionised water quickly, followed by three washes with PBS (5 minutes each).

6. Permeabilisation and blocking with blocking buffer (note 1.) for at least three hours.

7. Incubation with primary antibody solution (Table 1, note 2.) in PBS-S supplemented with 2.5% donkey serum overnight at 4°C. This incubation step can also be performed at room temperature for only a few hours.

8. Washing briefly with PBS-S (~1 minute) and then with blocking buffer thrice (10 minutes each).

9. Incubation with fluorescently-labelled secondary antibody solution (Table 2, note 2.) in PBS-S for two hours. To avoid bleaching of the fluorophores, the sections have to be shielded from light (for example using aluminium foil to wrap the plate) from this point on.

10. Washing with PBS-S twice (10 minutes each) and twice with PBS (10 minutes each).

11. Post fixation with 4% PFA in PBS for 30 minutes.

12. Washing with PBS supplemented with 100 mM glycine thrice (10 minutes each).

13. Sections were stored in Scale U2 buffer (Table 3) [40] at 4°C.

Super-resolution imaging

Optimal 'blinking' of the fluorophores can only be achieved in switching buffer (note 3.**Error!**

Reference source not found.). Therefore, stained samples should not be mounted on microscope slides

in mounting medium. Stained cells on glass coverslips are mounted in sample holder and covered with

buffer. Just prior to imaging, stained brain sections are mounted on glass coverslips.

1. Brain sections are set on top a No. 1.5 coverslip (25 mm in diameter, SLS #MIC3350) and let set

   to dry slightly. Care has to be taken to not completely dry out the tissue (Figure 1, A).

2. Melted 2% agarose is pipetted on top of the tissue to immobilize the brain sections (Figure 1, B).

   The porous agarose gel allows the switching buffer to penetrate the tissue. The agarose needs to

   dry and set before buffer is added.

3. The coverslip is then inserted into a 25 mm circular stage adaptor and imaging buffer (~1 ml)

   (note 3.) is pipetted on top (Figure 1, C). A smaller coverslip is used to seal the chamber.

Imaging Protocol

1. Using the CCD camera, a region of interest is selected by scanning the sample in standard

   epifluorescence mode (Figure 2, A and D).

2. Using the sCMOS camera and little laser power, the region of interest is confirmed for super-

   resolution imaging (Figure 2, B and E).

3. Photoswitching of the fluorophores is induced by greatly increasing the laser power to 0.6-6

   mW/μm^2.

4. An image series of several thousand (usually 30,000) frames is then recorded until most of the

   fluorophores have been recorded and blinking is diminished. Exposure/recording time should on

average match the time a single fluorophore emits photons (usually between 10 and 30 ms) to maximise signal-to-noise ratio and to not split the blinking over multiple frames.

5. The biplane mode of the Vutara microscope records a 3D image with a z range of 2 μm (note 4.). Nevertheless, by moving the piezo stage an image with a longer z range can be imaged.

6. During multi-colour imaging, channels should be recorded sequentially, and recording should start in the red range of the spectrum and end in the blue range to avoid bleaching and activating more than one fluorophore (note 5.).

Image Reconstruction and Visualisation

Experimental point spread function generation

An experimental point spread function (PSF) (note 6.) should be generated and used instead of a theoretical PSF to 1) fit the fluorophore localisations and 2) calibrate chromatic aberrations (note 5.). TetraSpeck beads (Thermo, #T7279) can be used to generate the experimental PSFs for the laser lines/fluorophores used. Fiducials are also included in the cell culture imaging preparations as reference points. As the beads fluoresce throughout the experiment they can easily be detected and traced to measure out mechanical drift of the sample.

1. Aliquot 1 μl TetraSpeck microspheres into a tube and sonicate for 10 minutes.

2. Add 500 μl dH$_2$O, vortex, sonicate again for 10 minutes and then vortex again.

3. Add 100 μl poly-DL-lysine solution (1 mg/ml) to the centre of a No. 1.5 coverglass. The coverslip should have the same quality and thickness as the ones used for imaging.

4. After 10 minutes aspirate the lysine solution and let the coverslip air dry.

5. Add 10-30 μl of the prepared 1:500 bead sample onto the centre of the dried lysine spot and let stand for 10 minutes and then aspirate the remaining solution.

6. Let sample air dry completely.

7. Aliquot 3-5 μl deionised water onto a glass slide and invert the coverslip on top.

8. Seal the coverslip with nail polish. The bead sample can also be used with the above mentioned circular stage adaptor. In that case, the bead sample does not have to be mounted but stored in PBS at 4°C. The imaging should also take place in PBS.

9. The experimental PSFs are then generated after a z stack (fifty 100 nm steps) of the TetraSpeck sample is imaged.

Image analysis

The raw data generated consists of several thousand frames and up to millions of PSFs (note 6.). The 3D localisation of every blinking event needs to be determined as accurately as possible, either by using commercial software (Vutara SRX; Figure 2, C and F) or one of the many freely available alternatives such as QuickPALM [44] or ThunderSTORM [45]. Most commonly, localisation algorithms fit a two- or three-dimensional Gaussian distribution at the centre of every detected fluorophore position and then sample the surrounding pixels (note 6.). Consequently, labelling density - sparse switching of fluorophores is desired to avoid overlapping of PSFs - and localization precision (number of photons/single fluorophore, pixel size, background signal/signal-to-noise ratio and emission wavelength) are important factors to consider when analysing experiments [46].

4. Notes

1.

The fixation of the specimen was done with PFA. However, other fixatives such as glutaraldehyde or methanol can also be used. Residual PFA needs to be removed from the sample as it autofluoresces and can introduce artefacts. Quenching of free PFA is done with $NaBH_4$ but NH_4Cl or glycine can also be used. When intracellular proteins are targeted the cells need to be permeabilised. To this end, we used

saponin, an amphipathic glycoside that acts as a mild detergent. In comparison to triton - the most commonly used detergent for permeabilisation - saponin reversibly permeabilises the cells and has to be added to every solution. Instead of saponin or triton, digitonin or leucoperm can be used. To prevent unspecific binding of the antibodies the specimen were blocked with normal donkey serum. The serum used should come from the same species in which the secondary antibodies were raised. Other blocking agents include bovine serum albumin or milk powder.

2.

Complexes of primary and secondary antibodies were used in the protocol described here. Thus, the detected localisations represent the position of the fluorophores rather than of the protein of interest, which might be ~15 nm further away. This localisation precision error can be avoided by directly tagging primary antibodies with fluorophores or by using smaller fragments of antibodies such as nanobodies [47], aptamers [48], monomeric streptavidin [49], or the pore-forming bacterial toxin streptolysin O [50,51]. Moreover, the protein of interest can also be modified directly with much smaller tags, e.g. hexa-histidine [52,53] or click chemistry approaches [54,55].

3.

The SMLM protocol described here is very similar to that of standard immunochemistry. However, it is essential that the organic dyes used exhibit photoswitching [56]. The blinking of the fluorophores is typically induced through thiols (mercaptoethylamine (MEA) or β-mercaptoethanol (β-ME)) in the switching buffer [57-59]. Different fluorophores exhibit different redox potentials and thus require different buffer compositions to ensure blinking. This can be particularly challenging in multicolour experiments [60,57] (note 6.).

4.

The procedure described here uses standard epifluorescence illumination. However, changing the angle of illumination can be useful to increase contrast. For example, when imaging cells, total internal reflection (TIR) illumination, or for thicker samples, highly inclined and laminated optical sheet (HILO)

illumination can be used [61]. Besides the biplane approach other methods exist for 3D imaging [61] such as astigmatism [62], double-helically arranged PSFs [63] or interferometry [64].

5.

Arguably the best and also most commonly used dye for dSTORM is Alexa647 [60,57]. It photoswitches easily and emits in the far-red spectrum, where tissue autofluorescence is comparatively low. When dual labelling is desired we recommend using Alexa647 in combination with CF568. Nevertheless, Cy3B or Alexa568 can also be used. In three colour experiments, Atto488 should be used in combination with the aforementioned dyes. Other options for multi-colour imaging are spectral demixing [65], which offers the advantage of negligible chromatic aberration [46] and multiplexed DNA-point accumulation for imaging in nanoscale topography (DNA-PAINT) [66].

6.

The intensity distribution in a diffraction-limited image that was taken with a conventional florescence microscope follows a PSF. The profile of a PSF can be fitted with a two- or three-dimensional Gaussian function with an uncertainty of only a few nanometres [67,68]. The diffraction limit of visible light typically lies at around 200–300 nm. This corresponds to the full width at half maximum (FWHM) of the PSF and depends on the emission wavelength and the number of detected photons. The PSFs of individual molecules overlap and cannot be distinguished as individual particles in standard fluorescence images in crowded biological samples. SMLM can separate the emission of fluorophores in space and time through photoactivation or –switching and hence can circumvent the diffraction limit [58,25,69,36]. The final SMLM image represents reconstructions of every detected, localised and fitted PSF.

5. References

1. Agulhon C, Petravicz J, McMullen AB, Sweger EJ, Minton SK, Taves SR, Casper KB, Fiacco TA, McCarthy KD (2008) What is the role of astrocyte calcium in neurophysiology? Neuron 59 (6):932-946. doi:10.1016/j.neuron.2008.09.004

2. Halassa MM, Haydon PG (2010) Integrated brain circuits: astrocytic networks modulate neuronal activity and behavior. Annual review of physiology 72:335-355. doi:10.1146/annurev-physiol-021909-135843

3. Seifert G, Carmignoto G, Steinhauser C (2010) Astrocyte dysfunction in epilepsy. Brain research reviews 63 (1-2):212-221. doi:10.1016/j.brainresrev.2009.10.004

4. Verkhratsky A, Sofroniew MV, Messing A, deLanerolle NC, Rempe D, Rodriguez JJ, Nedergaard M (2012) Neurological diseases as primary gliopathies: a reassessment of neurocentrism. ASN Neuro 4 (3). doi:10.1042/AN20120010

5. Volterra A, Meldolesi J (2005) Astrocytes, from brain glue to communication elements: the revolution continues. Nature reviews Neuroscience 6 (8):626-640. doi:10.1038/nrn1722

6. Bazargani N, Attwell D (2016) Astrocyte calcium signaling: the third wave. Nature neuroscience 19 (2):182-189. doi:10.1038/nn.4201

7. Khakh BS, Sofroniew MV (2015) Diversity of astrocyte functions and phenotypes in neural circuits. Nature neuroscience 18 (7):942-952. doi:10.1038/nn.4043

8. Rusakov DA (2015) Disentangling calcium-driven astrocyte physiology. Nature reviews Neuroscience 16 (4):226-233. doi:10.1038/nrn3878

9. Heller JP, Rusakov DA (2015) Morphological plasticity of astroglia: Understanding synaptic microenvironment. Glia 63 (12):2133-2151. doi:10.1002/glia.22821

10. Araque A, Carmignoto G, Haydon PG, Oliet SH, Robitaille R, Volterra A (2014) Gliotransmitters travel in time and space. Neuron 81 (4):728-739. doi:10.1016/j.neuron.2014.02.007

11. Zorec R, Araque A, Carmignoto G, Haydon PG, Verkhratsky A, Parpura V (2012) Astroglial excitability and gliotransmission: an appraisal of Ca2+ as a signalling route. ASN Neuro 4 (2). doi:10.1042/AN20110061

12. Rusakov DA, Bard L, Stewart MG, Henneberger C (2014) Diversity of astroglial functions alludes to subcellular specialisation. Trends in neurosciences 37 (4):228-242. doi:10.1016/j.tins.2014.02.008

13. Bernardinelli Y, Randall J, Janett E, Nikonenko I, Konig S, Jones EV, Flores CE, Murai KK, Bochet CG, Holtmaat A, Muller D (2014) Activity-dependent structural plasticity of perisynaptic astrocytic domains promotes excitatory synapse stability. Current biology : CB 24 (15):1679-1688. doi:10.1016/j.cub.2014.06.025

14. Haber M, Zhou L, Murai KK (2006) Cooperative astrocyte and dendritic spine dynamics at hippocampal excitatory synapses. The Journal of neuroscience : the official journal of the Society for Neuroscience 26 (35):8881-8891. doi:10.1523/JNEUROSCI.1302-06.2006

15. Hirrlinger J, Hulsmann S, Kirchhoff F (2004) Astroglial processes show spontaneous motility at active synaptic terminals in situ. The European journal of neuroscience 20 (8):2235-2239. doi:10.1111/j.1460-9568.2004.03689.x

16. Perez-Alvarez A, Navarrete M, Covelo A, Martin ED, Araque A (2014) Structural and functional plasticity of astrocyte processes and dendritic spine interactions. The Journal of neuroscience : the official journal of the Society for Neuroscience 34 (38):12738-12744. doi:10.1523/JNEUROSCI.2401-14.2014

17. Bernardinelli Y, Muller D, Nikonenko I (2014) Astrocyte-synapse structural plasticity. Neural plasticity 2014:232105. doi:10.1155/2014/232105

18. Theodosis DT, Poulain DA, Oliet SH (2008) Activity-dependent structural and functional plasticity of astrocyte-neuron interactions. Physiological reviews 88 (3):983-1008. doi:10.1152/physrev.00036.2007

19. Medvedev N, Popov V, Henneberger C, Kraev I, Rusakov DA, Stewart MG (2014) Glia selectively approach synapses on thin dendritic spines. Philosophical transactions of the Royal Society of London Series B, Biological sciences 369 (1654):20140047. doi:10.1098/rstb.2014.0047

20. Lushnikova I, Skibo G, Muller D, Nikonenko I (2009) Synaptic potentiation induces increased glial coverage of excitatory synapses in CA1 hippocampus. Hippocampus 19 (8):753-762. doi:10.1002/hipo.20551

21. Witcher MR, Kirov SA, Harris KM (2007) Plasticity of perisynaptic astroglia during synaptogenesis in the mature rat hippocampus. Glia 55 (1):13-23. doi:10.1002/glia.20415

22. Popov VI, Davies HA, Rogachevsky VV, Patrushev IV, Errington ML, Gabbott PL, Bliss TV, Stewart MG (2004) Remodelling of synaptic morphology but unchanged synaptic density during late phase long-term potentiation (LTP): a serial section electron micrograph study in the dentate gyrus in the anaesthetised rat. Neuroscience 128 (2):251-262. doi:10.1016/j.neuroscience.2004.06.029

23. Sherpa AD, Xiao F, Joseph N, Aoki C, Hrabetova S (2016) Activation of beta-adrenergic receptors in rat visual cortex expands astrocytic processes and reduces extracellular space volume. Synapse 70 (8):307-316. doi:10.1002/syn.21908

24. Witcher MR, Park YD, Lee MR, Sharma S, Harris KM, Kirov SA (2010) Three-dimensional relationships between perisynaptic astroglia and human hippocampal synapses. Glia 58 (5):572-587. doi:10.1002/glia.20946

25. Betzig E, Patterson GH, Sougrat R, Lindwasser OW, Olenych S, Bonifacino JS, Davidson MW, Lippincott-Schwartz J, Hess HF (2006) Imaging intracellular fluorescent proteins at nanometer resolution. Science 313 (5793):1642-1645. doi:10.1126/science.1127344

26. Huang B, Wang W, Bates M, Zhuang X (2008) Three-dimensional super-resolution imaging by stochastic optical reconstruction microscopy. Science 319 (5864):810-813. doi:10.1126/science.1153529

27. Klar TA, Jakobs S, Dyba M, Egner A, Hell SW (2000) Fluorescence microscopy with diffraction resolution barrier broken by stimulated emission. Proceedings of the National Academy of Sciences of the United States of America 97 (15):8206-8210

28. Heller JP, Rusakov DA (2017) The Nanoworld of the Tripartite Synapse: Insights from Super-Resolution Microscopy. Front Cell Neurosci 11:374. doi:10.3389/fncel.2017.00374

29. Panatier A, Arizono M, Nagerl UV (2014) Dissecting tripartite synapses with STED microscopy. Philosophical transactions of the Royal Society of London Series B, Biological sciences 369 (1654):20130597. doi:10.1098/rstb.2013.0597

30. Volterra A, Liaudet N, Savtchouk I (2014) Astrocyte Ca(2)(+) signalling: an unexpected complexity. Nature reviews Neuroscience 15 (5):327-335. doi:10.1038/nrn3725

31. Smith AJ, Verkman AS (2015) Superresolution Imaging of Aquaporin-4 Cluster Size in Antibody-Stained Paraffin Brain Sections. Biophysical journal 109 (12):2511-2522. doi:10.1016/j.bpj.2015.10.047

32. Gucek A, Jorgacevski J, Singh P, Geisler C, Lisjak M, Vardjan N, Kreft M, Egner A, Zorec R (2016) Dominant negative SNARE peptides stabilize the fusion pore in a narrow, release-unproductive state. Cellular and molecular life sciences : CMLS 73 (19):3719-3731. doi:10.1007/s00018-016-2213-2

33. Sakers K, Lake AM, Khazanchi R, Ouwenga R, Vasek MJ, Dani A, Dougherty JD (2017) Astrocytes locally translate transcripts in their peripheral processes. Proceedings of the National Academy of Sciences of the United States of America. doi:10.1073/pnas.1617782114

34. van de Linde S, Loschberger A, Klein T, Heidbreder M, Wolter S, Heilemann M, Sauer M (2011) Direct stochastic optical reconstruction microscopy with standard fluorescent probes. Nat Protoc 6 (7):991-1009. doi:10.1038/nprot.2011.336

35. Endesfelder U, Heilemann M (2015) Direct stochastic optical reconstruction microscopy (dSTORM). Methods in molecular biology 1251:263-276. doi:10.1007/978-1-4939-2080-8_14

36. Heilemann M, van de Linde S, Schuttpelz M, Kasper R, Seefeldt B, Mukherjee A, Tinnefeld P, Sauer M (2008) Subdiffraction-resolution fluorescence imaging with conventional fluorescent probes. Angew Chem Int Ed Engl 47 (33):6172-6176. doi:10.1002/anie.200802376

37. Oberheim NA, Goldman SA, Nedergaard M (2012) Heterogeneity of astrocytic form and function. Methods in molecular biology 814:23-45. doi:10.1007/978-1-61779-452-0_3

38. Grosche A, Grosche J, Tackenberg M, Scheller D, Gerstner G, Gumprecht A, Pannicke T, Hirrlinger PG, Wilhelmsson U, Huttmann K, Hartig W, Steinhauser C, Pekny M, Reichenbach A (2013) Versatile

and simple approach to determine astrocyte territories in mouse neocortex and hippocampus. PloS one 8 (7):e69143. doi:10.1371/journal.pone.0069143

39. Heller JP, Michaluk P, Sugao K, Rusakov DA (2017) Probing nano-organization of astroglia with multi-color super-resolution microscopy. Journal of neuroscience research. doi:10.1002/jnr.24026

40. Hama H, Kurokawa H, Kawano H, Ando R, Shimogori T, Noda H, Fukami K, Sakaue-Sawano A, Miyawaki A (2011) Scale: a chemical approach for fluorescence imaging and reconstruction of transparent mouse brain. Nature neuroscience 14 (11):1481-1488. doi:10.1038/nn.2928

41. Juette MF, Gould TJ, Lessard MD, Mlodzianoski MJ, Nagpure BS, Bennett BT, Hess ST, Bewersdorf J (2008) Three-dimensional sub-100 nm resolution fluorescence microscopy of thick samples. Nat Methods 5 (6):527-529. doi:10.1038/nmeth.1211

42. Mlodzianoski MJ, Juette MF, Beane GL, Bewersdorf J (2009) Experimental characterization of 3D localization techniques for particle-tracking and super-resolution microscopy. Opt Express 17 (10):8264-8277

43. Metcalf DJ, Edwards R, Kumarswami N, Knight AE (2013) Test samples for optimizing STORM super-resolution microscopy. J Vis Exp (79). doi:10.3791/50579

44. Henriques R, Lelek M, Fornasiero EF, Valtorta F, Zimmer C, Mhlanga MM (2010) QuickPALM: 3D real-time photoactivation nanoscopy image processing in ImageJ. Nat Methods 7 (5):339-340. doi:10.1038/nmeth0510-339

45. Ovesny M, Krizek P, Borkovec J, Svindrych Z, Hagen GM (2014) ThunderSTORM: a comprehensive ImageJ plug-in for PALM and STORM data analysis and super-resolution imaging. Bioinformatics 30 (16):2389-2390. doi:10.1093/bioinformatics/btu202

46. Herrmannsdorfer F, Flottmann B, Nanguneri S, Venkataramani V, Horstmann H, Kuner T, Heilemann M (2017) 3D d STORM Imaging of Fixed Brain Tissue. Methods in molecular biology 1538:169-184. doi:10.1007/978-1-4939-6688-2_13

47. Pleiner T, Bates M, Trakhanov S, Lee CT, Schliep JE, Chug H, Bohning M, Stark H, Urlaub H, Gorlich D (2015) Nanobodies: site-specific labeling for super-resolution imaging, rapid epitope-mapping and native protein complex isolation. Elife 4:e11349. doi:10.7554/eLife.11349

48. de Castro MA, Rammner B, Opazo F (2016) Aptamer Stainings for Super-resolution Microscopy. Methods in molecular biology 1380:197-210. doi:10.1007/978-1-4939-3197-2_17

49. Chamma I, Rossier O, Giannone G, Thoumine O, Sainlos M (2017) Optimized labeling of membrane proteins for applications to super-resolution imaging in confined cellular environments using monomeric streptavidin. Nat Protoc 12 (4):748-763. doi:10.1038/nprot.2017.010

50. Teng KW, Ishitsuka Y, Ren P, Youn Y, Deng X, Ge P, Belmont AS, Selvin PR (2016) Labeling proteins inside living cells using external fluorophores for microscopy. Elife 5. doi:10.7554/eLife.20378

51. Teng KW, Ishitsuka Y, Ren P, Youn Y, Deng X, Ge P, Lee SH, Belmont AS, Selvin PR (2017) Labeling Proteins Inside Living Cells Using External Fluorophores for Fluorescence Microscopy. Elife 6. doi:10.7554/eLife.25460

52. Wieneke R, Raulf A, Kollmannsperger A, Heilemann M, Tampe R (2015) SLAP: Small Labeling Pair for Single-Molecule Super-Resolution Imaging. Angew Chem Int Ed Engl 54 (35):10216-10219. doi:10.1002/anie.201503215

53. Lotze J, Reinhardt U, Seitz O, Beck-Sickinger AG (2016) Peptide-tags for site-specific protein labelling in vitro and in vivo. Mol Biosyst 12 (6):1731-1745. doi:10.1039/c6mb00023a

54. Raulf A, Spahn CK, Zessin PJ, Finan K, Bernhardt S, Heckel A, Heilemann M (2014) Click chemistry facilitates direct labelling and super-resolution imaging of nucleic acids and proteinsdaggerElectronic supplementary information (ESI) available. See DOI: 10.1039/c4ra01027bClick here for additional data file. RSC Adv 4 (57):30462-30466. doi:10.1039/c4ra01027b

55. Mateos-Gil P, Letschert S, Doose S, Sauer M (2016) Super-Resolution Imaging of Plasma Membrane Proteins with Click Chemistry. Front Cell Dev Biol 4:98. doi:10.3389/fcell.2016.00098

56. Furstenberg A, Heilemann M (2013) Single-molecule localization microscopy-near-molecular spatial resolution in light microscopy with photoswitchable fluorophores. Phys Chem Chem Phys 15 (36):14919-14930. doi:10.1039/c3cp52289j

57. Dempsey GT, Vaughan JC, Chen KH, Bates M, Zhuang X (2011) Evaluation of fluorophores for optimal performance in localization-based super-resolution imaging. Nat Methods 8 (12):1027-1036. doi:10.1038/nmeth.1768

58. Rust MJ, Bates M, Zhuang X (2006) Sub-diffraction-limit imaging by stochastic optical reconstruction microscopy (STORM). Nat Methods 3 (10):793-795. doi:10.1038/nmeth929

59. Chozinski TJ, Gagnon LA, Vaughan JC (2014) Twinkle, twinkle little star: photoswitchable fluorophores for super-resolution imaging. FEBS Lett 588 (19):3603-3612. doi:10.1016/j.febslet.2014.06.043

60. Turkowyd B, Virant D, Endesfelder U (2016) From single molecules to life: microscopy at the nanoscale. Anal Bioanal Chem 408 (25):6885-6911. doi:10.1007/s00216-016-9781-8

61. Herbert S, Soares H, Zimmer C, Henriques R (2012) Single-molecule localization super-resolution microscopy: deeper and faster. Microsc Microanal 18 (6):1419-1429. doi:10.1017/S1431927612013347

62. Kao HP, Verkman AS (1994) Tracking of single fluorescent particles in three dimensions: use of cylindrical optics to encode particle position. Biophysical journal 67 (3):1291-1300. doi:10.1016/S0006-3495(94)80601-0

63. Pavani SR, Thompson MA, Biteen JS, Lord SJ, Liu N, Twieg RJ, Piestun R, Moerner WE (2009) Three-dimensional, single-molecule fluorescence imaging beyond the diffraction limit by using a double-helix point spread function. Proceedings of the National Academy of Sciences of the United States of America 106 (9):2995-2999. doi:10.1073/pnas.0900245106

64. Shtengel G, Galbraith JA, Galbraith CG, Lippincott-Schwartz J, Gillette JM, Manley S, Sougrat R, Waterman CM, Kanchanawong P, Davidson MW, Fetter RD, Hess HF (2009) Interferometric fluorescent super-resolution microscopy resolves 3D cellular ultrastructure. Proceedings of the National Academy of Sciences of the United States of America 106 (9):3125-3130. doi:10.1073/pnas.0813131106

65. Lampe A, Haucke V, Sigrist SJ, Heilemann M, Schmoranzer J (2012) Multi-colour direct STORM with red emitting carbocyanines. Biol Cell 104 (4):229-237. doi:10.1111/boc.201100011

66. Jungmann R, Avendano MS, Woehrstein JB, Dai M, Shih WM, Yin P (2014) Multiplexed 3D cellular super-resolution imaging with DNA-PAINT and Exchange-PAINT. Nat Methods 11 (3):313-318. doi:10.1038/nmeth.2835

67. Smith CS, Joseph N, Rieger B, Lidke KA (2010) Fast, single-molecule localization that achieves theoretically minimum uncertainty. Nat Methods 7 (5):373-375. doi:10.1038/nmeth.1449

68. Thompson RE, Larson DR, Webb WW (2002) Precise nanometer localization analysis for individual fluorescent probes. Biophysical journal 82 (5):2775-2783. doi:10.1016/S0006-3495(02)75618-X

69. Hess ST, Girirajan TP, Mason MD (2006) Ultra-high resolution imaging by fluorescence photoactivation localization microscopy. Biophysical journal 91 (11):4258-4272. doi:10.1529/biophysj.106.091116

Figure captions

Figure 1: Tissue preparation for super-resolution imaging.

(A) The brain section is placed on top of a coverslip. **(B)** Warmed 2% agarose is used to immobilize the tissue. **(C)** The imaging chamber is filled with buffer (note **Error! Reference source not found.**). The arrows are pointing at the tissue.

Figure 2: Super-resolution imaging of astrocytes *in vitro*.

(A) Wide-field image of astrocytes in rat mixed cortical cultures expressing GFAP. **(B)** Higher magnification image of area shown by rectangle in A, wide-field fluorescence mode. **(C)** SMLM image of area shown in B. Scale bars = 5 µm.

Figure 3: Super-resolution imaging of astrocytes *in situ*.

(A) Wide-field image of astrocytes in mouse brain sections expressing GFAP. **(B)** Higher magnification image of area shown by rectangle in A, wide-field fluorescence mode. **(C)** SMLM image of area shown in B. **(D)** Widefield image of S100β in the same field of view as in A. **(E)** Higher magnification image of area shown by rectangle in D, wide-field fluorescence mode. **(F)** SMLM image of area shown in E. **(G)** Merged image of B and E, with GFAP shown in green and S100β in magenta. **(H)** Merged image of C and F, with GFAP shown in green and S100β in magenta. Scale bars = 5 µm.

Tables

Table 1: Primary antibodies used.

RRID = Research Resource Identifier, ICC = Dilution factor used in immunocytochemistry, IHC =

Dilution factor used in immunohistochemistry

Antigen	host	Clone	Supplier	product code	RRID	ICC	IHC
GFAP	Mouse	GA5	Novus	NBP2-29415	AB_2631231	1:500	1:500
S100β	Rabbit	Polyclonal	Synaptic systems	287 003	AB_2620024	1:200	1:200

Table 2: Secondary antibodies used.

Ig = Immunoglobulin, RRID = Research Resource Identifier, ICC = Dilution factor used in

immunocytochemistry IHC = Dilution factor used in immunohistochemistry

Antigen	Feature	Host	Supplier	product code	RRID	ICC	IHC
Mouse IgG	CF568-conjugated	Donkey	Biotium	20105	AB_10557030	1:200	1:200
Rabbit IgG	Alexa647-conjugated	Goat	Thermo	A21245	AB_2535813	1:500	1:500

Table 3: Scale U2 buffer [40]. This buffer clears the tissue with minimal to no extension to minimise

autofluorescence [40].

Ingredient	Concentration	Supplier and product code
Urea	4 M	Sigma, #U6504
Glycerol	30%	Fisher, #BP229-1
Triton X-100	0.1%	Sigma, #T9284

Table 4: Photoswitching buffer [43].

Enzyme Stock Solution (A)		
Ingredient	Concentration	Supplier and product number

10 µl catalase	20 µg/ml	Sigma, #C40
20 µl 1M TCEP	4 mM	Sigma, #C4706
2.5 ml glycerol	50%	Fisher, #BP229-1
125 µl 1M KCl	25 mM	Sigma, #P9333
100 µl 1M Tris-HCl pH 7.5	20 mM	Sigma, #33742
5 mg glucose oxidase	1 mg/ml	Sigma, #G2133

Top up to 5 ml with distilled water and dispense into 50 µl aliquots and store frozen at -20°C (for up to one year).

Glucose Stock Solution (B)

Ingredient	Concentration	supplier and product number
4 g glucose	100 mg/ml	Sigma, #G8270
4 ml glycerol	10%	Fisher, #BP229-1

Top up to 40 ml with distilled water and dispense into 400 µl aliquots and store at -20°C (for up to one year).

Reducing Agent Stock Solution (C)

Ingredient	Concentration	supplier and product number
113.6 mg MEA-HCl	1 M	Sigma, #M6500

Top up to 1 ml with distilled water and store at 4°C on the day of imaging. This solution can also be prepared in advance and stored at -20°C for up to one year (do not refreeze).

Just prior to imaging mix the above solutions in the following ratio:

50 µl Solution A

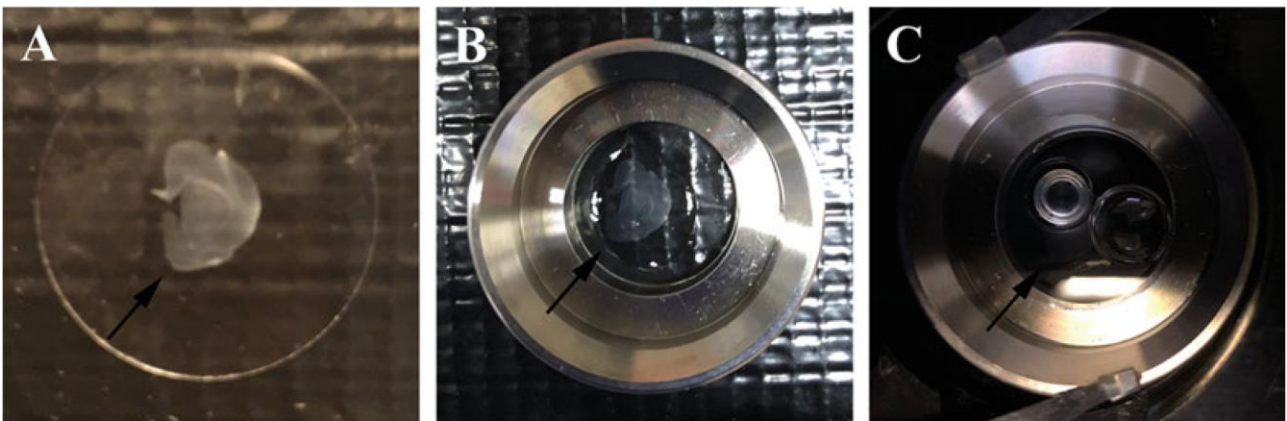400 µl Solution B

100 µl Solution C

450 µl PBS

Fig. 1 Tissue preparation for super-resolution imaging. (**a**) The brain section is placed on top of a coverslip. (**b**) Warmed 2% agarose is used to immobilize the tissue. (**c**) The imaging chamber is filled with buffer (*see* **Note 3**), and a coverslip is used to seal the chamber. The arrows are pointing toward the tissue
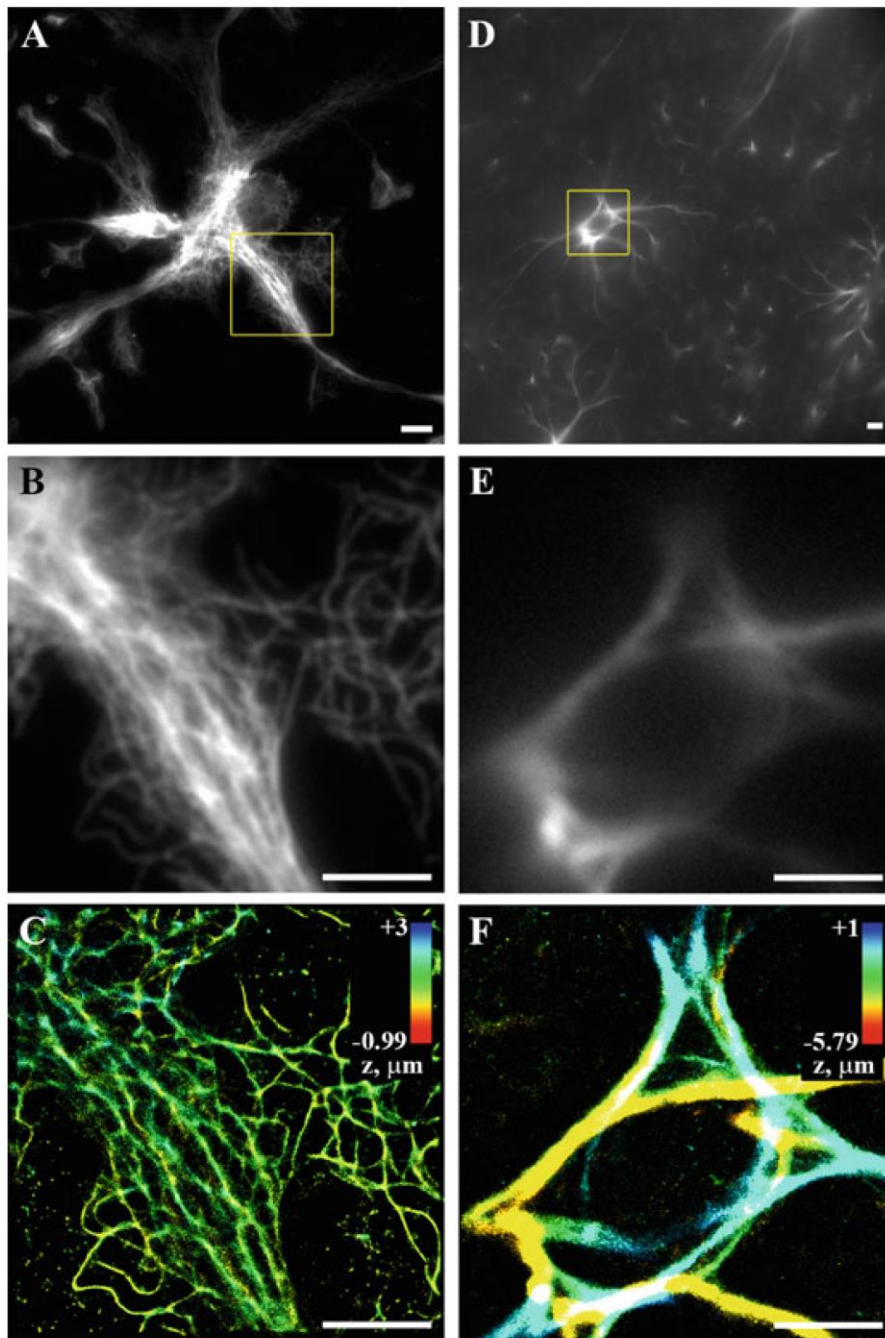
Fig. 2 Super-resolution imaging of astrocytes in vitro and in situ. (**a**) Wide-field image of astrocytes in rat mixed cortical cultures expressing GFAP (Alexa 647-tagged). (**b**) Higher magnification image of area shown by rectangle in **a**, wide-field fluorescence mode. (**c**) SMLM image of area shown in **b**. (**d**) Wide-field image of astrocytes in rat brain sections expressing GFAP (Alexa 647-tagged). (**e**) Higher magnification image of area shown by rectangle in **d**, wide-field fluorescence mode. (**f**) SMLM image of area shown in **e**. Scale bars = 5 μm
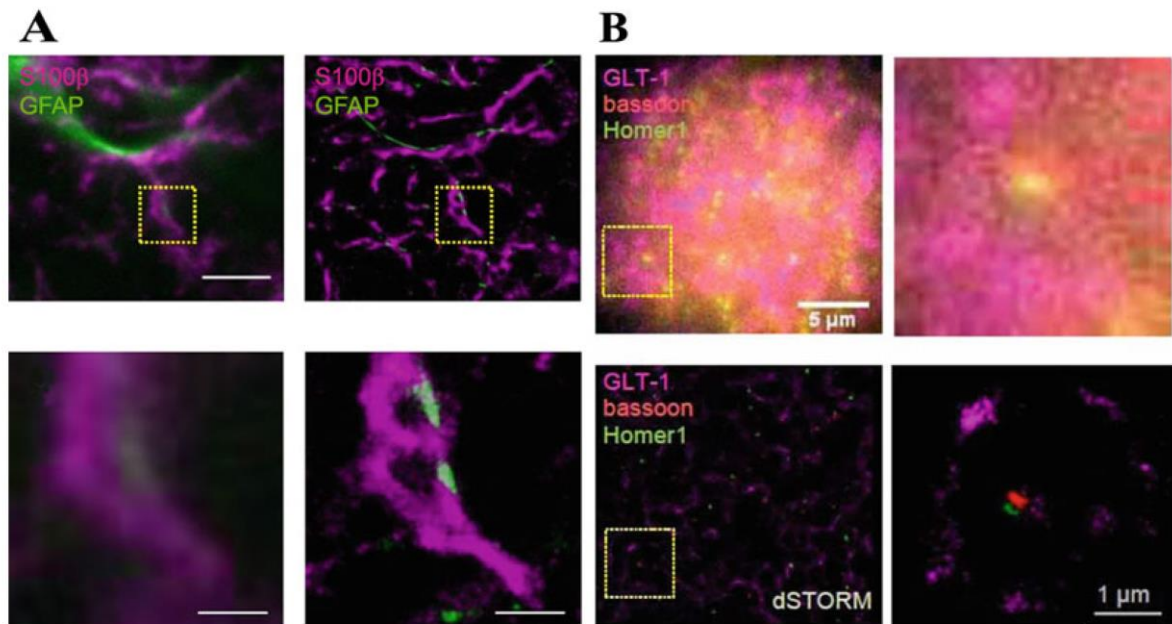
Fig. 3 Super-resolution imaging of astrocytes and tripartite synapses in situ. (**a**) Nanoscopy of S100β (magenta, Alexa 647-tagged) in GFAP (green, CF568-tagged)-expressing cells in rat brain tissue sections. Wide-field (left) and SMLM (right) images of astrocyte compartments in brain tissue sections at lower (top) and higher (bottom) magnification; dotted squares (top), magnified area. Scale bars: 5 μm (top) and 1 μm (bottom). Reproduced from [39] with permission. (**b**) Nanoscopy of tripartite synapses in rat brain sections. Wide-field (top) and SMLM (bottom) images of glutamate transporter GLT-1 (magenta, Alexa 647-tagged), bassoon (red, CF568-tagged) and Homer1 (green, Atto 488-tagged) at lower (left) and higher (right) magnification; dotted squares (left), magnified area. Scale bars: 5 μm (left) and 1 μm (right). Reproduced from [28] with permission